Materials & Design 245 (2024) 113230

Contents lists available at ScienceDirect

Materials & Design

journal homepage: www.elsevier.com/locate/matdes

A detailed investigation of acetylated cellulose nanofiber films as a substrate for printed electronics

Jenny Wiklund [a,b,*], Arttu Miettinen [c,d], Joni Parkkonen [c], Lauri Mela [b], Alp Karakoç [b], Jouni Paltakari [a]

[a] Department of Bioproducts and Biosystems, Aalto University, Vuorimiehentie 1, Espoo, 02150, Finland
[b] Department of Information and Communications Engineering, Aalto University, Maarintie 8, Espoo, 02150, Finland
[c] Department of Physics, Nanoscience Center, and School of Resource Wisdom, University of Jyväskylä, Jyväskylä, 40014, Finland
[d] Department of Engineering, Mathematics and Science Education, Mid Sweden University, Sundsvall, 85170, Sweden

ARTICLE INFO

Keywords:
Acetylation
Nanocellulose
Printed electronics
Print quality
Electrical properties
Mechanical properties

ABSTRACT

The increased interest in printed electronics necessitates the development of suitable sustainable substrates for them. In this study, the suitability of acetylated cellulose nanofiber (ACNF) films as substrates for printed electronics were examined through (I) the ink-substrates interaction, (II) print quality, and (III) electrical and (IV) mechanical properties of the printed pattern on the ACNF substrates. The results have been compared with cellulose nanofiber (CNF) and commercial reference material (CRM) substrates. The wetting of the silver nanoparticle (AgNP) ink on the ACNF substrate was found out to be excellent. The thickness of the printed pattern increased and the hole area fraction decreased with each consecutive layer of ink. The comparative investigations demonstrated that the electrical properties of the printed patterns were almost as good for 4 layers of ink on the ACNF substrate (1.6 Ω resistance) as the ones on the CRM substrate (1.2 Ω resistance). Additionally, the printed pattern on the ACNF substrate endured the adhesion and bending tests significantly better compared to the CRM substrate. Therefore, this study demonstrates that ACNF substrates could be a suitable candidate for printed electronics, which are more sustainable yet with similar functionalities in comparison with the conventional fossil based substrates.

1. Introduction

The topic of printed electronics has attracted a lot of attention in the past decades for several reasons. Printing is a more environmentally friendly approach for producing electronics compared to the conventional subtractive manufacturing methods. Due to the reduction of non-renewable resource waste and on-demand material utilization, printing processes meet the sustainability goals [1,2]. Additionally, printing, such as ink- and aerosol-jet printing, enables the production of tailor-made designs and small-scale manufacturing at low cost [3,4]. Manufacturing electronics using non-contact printing and inks with low temperature sintering also provides a great freedom for the use of a wide variety of substrates that can easily degrade when exposed to high sintering temperatures [5,6].

The substrate is the base of an electronic device. It separates electric devices from each other, like an electric insulator. The substrates traditionally used in electronics are commonly high-performance, stiff and non-degradable over time [7]. Due to their fragility, they are not suitable to be used in flexible electronics or implants [8]. Depending on the application for the printed electronic device the requirements on the substrate can vary significantly. Rigidity, surface smoothness, non-porosity, flexibility, transparency, non-toxicity, heat resistance, low thermal expansion, recyclability or biodegradability, light weight, thickness and low cost are some of the properties, which can be important to consider, when designing a suitable substrate for different printed electronic devices [9–12,1].

The most used substrate for traditional printing is paper made from cellulose [13,14]. Cellulose is a low-cost, non-toxic, renewable resource,

* Corresponding author at: Department of Bioproducts and Biosystems, Aalto University, Vuorimiehentie 1, Espoo, 02150, Finland.
E-mail addresses: jenny.wiklund@aalto.fi (J. Wiklund), arttu.i.miettinen@jyu.fi (A. Miettinen), joni.parkkonen@jyu.fi (J. Parkkonen), lauri.mela@aalto.fi (L. Mela), alp.karakoc@alumni.aalto.fi (A. Karakoç), jouni.paltakari@aalto.fi (J. Paltakari).

https://doi.org/10.1016/j.matdes.2024.113230
Received 21 February 2024; Received in revised form 18 July 2024; Accepted 5 August 2024
Available online 10 August 2024

and has been widely used for over 2000 years in various applications due to its many attractive qualities i.e., flexibility, good processability, biocompatibility and biodegradability. However, paper can be very challenging to use as a substrate for printed electronics, due to its absorptive nature, high porosity and surface roughness [15].

These challenges can for example be overcome by printing multiple layers of conductive ink [16], or by coating the paper [17]. The spectrum of properties can also be improved by using cellulose in nanoscale i.e., nanocellulose (NC), which simply broadens its functionalities and the range of applications. When designing a NC based substrates, some of the properties of the substrate have to be taken into account, such as chemical composition, surface energy, surface roughness, porosity and absorption of the ink [18]. A substrate with a higher surface roughness and porosity will need more layers of ink to achieve the same electrical properties compared to a smoother and less porous substrate. This will increase the amount of used ink, which often is made from non-renewable resources.

Based on the specific applications or characteristics of the ink used, NC based substrates can be modified and designed as hydrophobic, transparent, smooth, and strong platforms for recyclable printed electronics [19,20]. There are three main groups of NC, cellulose nanofibers (CNF), cellulose nanocrystals (CNC) and bacterial cellulose (BC). These NC groups differ from each other in how they are produced, as well as their surface chemistries, crystallinities, and mechanical properties [21]. The highly crystalline CNC is mainly produced using acid hydrolysis, while BC is extracted using microorganisms [22]. CNF can be produced using mechanical pretreatments, such as grinding, milling and homogenization, or/and chemical pretreatments, such as 2,2,6,6-tetramethylpiperidine-1-oxyl radical (TEMPO) oxidation or acetylation.

Acetylation of cellulose has drawn a lot of interest both industrially and scientifically, because it is a green scalable approach, with an established chemistry [23,24]. During the acetylation of CNF, the hydroxyl (OH) groups in the glucose chains are substituted with acetyl ($COCH_3$) groups [25–29]. The acetylation can be done either before or after the mechanical treatment of the fibers. This process reduces the interaction forces between the fibers and improves the hydrophobicity, thermal degradation, dispersive and optical properties of the acetylated CNF (ACNF) films and therefore makes them a viable alternative as a substrate for printed electronics.

Additionally, inkjet printing electronics on ACNF substrates would be a more environmentally friendly approach compared to the conventional subtractive manufacturing method with fossil based substrates. The use of ACNF as a potential substrate in printed electronics has been studied by e.g. Yang et al. [28], and in a composite with a transparent polymer by Yagyu et al. [27]. Yang et al. [28] studied the thermal properties, tensile strength and light transmittance of ACNF, in order to evaluate its suitability as a substrate. Compared with other methods of modifying CNF, ACNF is commonly used in order to improve the hydrophobicity [30], dispersive behavior [31], thermal [32] and dimensional stability [33] of the film.

In this study, the suitability of ACNF films as substrates for printed electronics is evaluated by investigating the interaction between silver nanoparticle (AgNP) ink and ACNF films. Additionally, the print quality, electrical and mechanical properties of the printed patterns on the substrates are studied. The results are compared to the results of CNF and commercial reference material (CRM) films, when applicable.

2. Materials and methods

Materials. For the CNF and ACNF dried bleached birch cellulose was used. Additionally the following chemicals were used: hydrochloric acid (HCl, 0.01 M), sodium bicarbonate ($NaHCO_3$, 0.005 M), acetone (CH_3COCH_3, AnalaR NORMAPUR®, ≥99.8%), anhydrous glacial acetic acid (H_3CCOOH, EMPARTA®, 100%), toluene ($C_6H_5CH_3$, AnalaR NORMAPUR®, ≥99.5%), sulfuric acid (H_2SO_4, EMSURE®, 95-97%) and sodium hydroxide (NaOH, EMSURE®, 50%). All chemicals were acquired from Sigma Aldrich. Deionized water was used throughout the experiments. Novele™, polyethylene terephthalate (PET)-based, substrates were obtained from Novacentrix® as a CRM [34–36]. The AgNP ink used in the experiments was Metalon® JS-A191 from NovaCentrix®. The reported surface tension, density and viscosity of the ink were 29.9 mN/m, 1.61 g/cm^3 and 12.8 mPa·s, respectively.

Preparation of CNFs. Dried bleached birch cellulose was soaked in water overnight and beaten into a 1.5 wt% slurry using a Hollander beater for 30 min. Sodium washing was used to deionize the birch pulp slurry. The excess water was removed from the slurry using a pressure suction filtrate machine with a 10 μm filter. A mix of deiniozed water with 0.72 wt% pulp and 3.6×10^{-4} wt% 0.01 M hydrochloric acid was blended with a whisker for 15 minutes. The excess liquid was filtrated and the pulp was rinsed and soaked for 10-15 min with deionized water twice. Deionized water was mixed with 0.72 wt% pulp and 2.1×10^{-4} wt% 0.005 M sodium bicarbonate, while mixing with a whisker sodium hydroxide was added until a pH of 9.5-10 was reached and further mixed for 15 min. The blend was then filtrated and rinsed until the conductivity was less than 20 μS/cm. Finally the excess water was filtrated. The deionized pulp was mixed with water until it had a wt% of 1. A Supermasscolloider (Masuko) was used to grind the pulp slurry seven times, until it had a gel-like composition. The final CNF was obtained by further disintegrating the pulp using a Microfluidizer (M-110P, Microfluidics In., Newton, MA) three times. CNF films with a grammage of 60 g/m^2 were cast dried from the 0.5 wt% suspension in petri dishes.

Preparation of ACNFs. CNF with a dry weight of 10 g was acetylated in order to produce ACNF. The acetylation process involved two solvent exchanges as pretreatments. The first solvent exchange was from water to acetone, by removing the water using a Thermo Scientific SL40FR centrifuge and then soaking the CNF in acetone for 30 min while magnetically stirring and repeat twice. The second solvent exchange was from acetone to anhydrous glacial acetic acid, by removing the acetone using a centrifuge and then soaking the CNF in anhydrous acetic acid for 1 h while magnetically stirring. The anhydrous glacial acetic acid was removed by centrifuging. The CNF was added to a mixed solution of 250 ml toluene, 200 ml anhydrous glacial acetic acid, 1 ml sulfuric acid and magnetically stirred for 10 min, 60 ml of additional anhydrous glacial acetic acid was added while stirring. The acetylation process was performed while magnetically stirring for 3 h. The ACNF mass was washed and centrifuged several times using deionized water. Finally, a small amount of sodium hydroxide was added in order to increase the pH to 6-8 prior to the final washing of the mass and water was added to get a 0.65 wt% ACNF suspension. ACNF films were obtained by cast drying the suspension in petri dishes in order to achieve a grammage of 60 g/m^2 for the thin films.

Inkjet printing. A Fujifilm Dimatix Materials Printer DMP-2831 was used to print patterns with the AgNP ink on the substrates using a cartridge with a drop volume of 10 pl. The AgNP ink was chosen for printing, due to its suitable surface tension and viscosity for the printer [37–39]. The jetting voltage and drop spacing used for printing are 22-28 V and 25 μm, respectively. A delay time of 5 min was used between the layers, when printing multiple layers. A Xenon flash-lamp system (t = 30 seconds) and an oven (140 °C, 15 minutes) were used for the sintering of the AgNP ink after printing.

Characterization of ink - substrate interaction. Theta Flex optical tensiometer was used to measure the surface energy, surface tension and contact angle (CA). The CA of deionized water, di-iodomethane and glycerol on the surface of CNF, ACNF and CRM films was measured for 10 seconds using sessile drop measurement in order to calculate the surface energy of the substrates. The software OneAttension used the $Owens-Wendt-Rabel\&Kaelble$ (OWRK) model to calculate the surface energy of the substrates. The surface tension of the ink was measured using pendant drop measurements for 10 seconds. The CA of the ink on the substrates were measured for 300 seconds using sessile drop measurements. A drop volume of 3-5 μl was used in the measurements. The CA measurements were made without sintering.

Characterization of print quality. An optical microscope (Olympus SZX10) was used to analyze the quality of the printed pattern and the spreading of the ink on the substrate after sintering. The printed pattern for the optical microscope consisted of 1-4 layers of ink and was 20 mm long and 0.1 mm, 0.3 mm, 0.5 mm, 0.7 mm and 0.9 mm wide.

X-ray microtomography was applied in characterization of the thickness and roughness of the printed patterns, and the roughness of only the ACNF and CRM substrates. It was deemed unnecessary to do the measurements for the CNF substrate, due to its poor electrical properties. Sample of approximately 1 mm × 2 mm of each material was imaged using Xradia microXCT-400 device (Xradia, Concord, California, USA) with 1.1 μm pixel size. X-ray tube acceleration voltage was set to 50 kV and power to 4 W, and 1900 projection images over 190° of sample rotation were collected with 8 s exposure time each. The projection images were reconstructed into three-dimensional volume images using the pi2[1] software.

The reconstructions were cropped to remove unnecessary empty space around the sample, and the surfaces of the prints and the substrates were found using the Carpet algorithm [40]. There, an interface between two materials is defined as the converged position of a soft carpet-like surface following specific Edwards-Wilkinson dynamics. The result of the method is a height of the interface above some datum as a function of lateral position, i.e., a height map. The thickness of the printed layer was then defined as the difference of its top and bottom surface height maps. Holes in the print were defined by locations where thickness was zero or negative.

In order to characterize the roughness of the printed surface and the roughness of the substrate surface, the corresponding height maps were first high-pass filtered ($\sigma = 33\,\mu m$) to remove height variations caused by the global curvature of the sample. Then, the mean value of the filtered height map was subtracted from it, resulting in a surface roughness map. Finally, the mean absolute height (Sa) and the root mean squared (RMS) height (Sq) of the map were calculated in order to characterize the differences in roughness of the surfaces.

Image analysis was performed with the pi2 software.

Characterization of electrical properties. The resistance of the printed patterns were measured using Fluke 789 multimeter. The length and width of the printed pattern was 50 mm and 1 mm, respectively, with 5 mm squared measurement pads in both ends. The pattern was printed on CNF, ACNF and CRM substrates with 1-4 layers. The sheet resistance was measured using the Ossila Four-Point Probe System from a pattern, 40 mm long and 30 mm wide with 4 layers printed on ACNF and CRM.

The relative permittivity was estimated using the differential phase length method [41]. Two transmission lines ($l_1 = 40\,mm$, $l_2 = 80\,mm$) with coplanar waveguide (CPW) geometry were printed on the ACNF substrate and then measured for their phase response as a function of frequency. A pair of measurement probes, which consist of an SMA connector with soldered pogo pins, were attached to adjustable micrometer platforms. Through these probes the ends of the transmission lines were connected to a vector network analyzer (R&S ZNB8) for measuring the phase response. The substrate was supported by a 3-D printed platform ensuring that the immediate environment above and below the substrate was air. The effective permittivity ε_{eff} is expressed as

$$\varepsilon_{eff} = \left(\frac{\Delta\phi c}{2\pi f \Delta L} \right)^2, \quad (1)$$

where $\Delta\phi$ is the difference between the unwrapped phase responses of the lines, c is speed of light in vacuum, f is frequency and ΔL is length difference of the lines. The relationship between ε_{eff} and the substrate's relative permittivity ε_r depends on the exact geometry of the line. ε_r was determined by using an electromagnetic (EM) simulation of the line geometry with Keysight ADS LineCalc program and iterating different values for ε_r until the simulated ε_{eff} matches the value from measurement.

[1] Freely available at https://github.com/arttumiettinen/pi2.

Table 1
The surface energy measurements for cellulose nanofiber (CNF), acetylated cellulose nanofiber (ACNF) and commercial reference material (CRM) films. The initial (t = 0 s) and final (t = 300 s) contact angle (CA) for the silver nanoparticle (AgNP) ink on CNF, ACNF and CRM.

	Cellulose nanofiber (CNF)	Acetylated cellulose nanofiber (ACNF)	Commercial reference material (CRM)
γ^{tot} (mN/m)	31.31	43.43	40.93
γ^{d} (mN/m)	29.41	28.56	36.98
γ^{p} (mN/m)	1.90	14.87	3.95
Initial CA (°)	33.34	14.3	57.98
Final CA (°)	19.71	6.28	48.48

Characterization of Mechanical properties. The adhesion of the printed pattern on the ACNF and CRM substrate was tested using a tape adhesion test, using 3M 811 Removable tape (width 19 mm). A pattern, with a length and width of 40 mm and 30 mm, respectively, was printed onto the substrates in four layers of ink. The printed substrates were glued to a cardboard using tape, covering some of the printed pattern. A piece of tape was firmly pressed onto the printed pattern on the substrates. The tape adhesion test was performed by slowly peeling the tape off at a 90° angle. Before and after the test, the sheet resistance was measured using Ossila Four-Point Probe measurement device and images of the printed area were taken using an optical microscope (Olympus SZX10) and a camera.

A Bending Tester *L&W* SE 160 was used to measure the bending resistance of the ACNF and CRM substrates with a printed pattern. The width and length of the substrates were 38 mm and 80 mm, respectively. The bending angle and length used were 30° and 50 mm, respectively. The pattern was printed using four layers of ink and the length and width of the pattern was 40 mm and 1 mm, respectively, with 5 mm squared measurement pads in both ends. The resistance was measured using a multimeter after each test. After 10 bending measurements with a 30° angle, the settings were changed to creasing in order to achieve an 90° angle.

3. Results and discussion

3.1. Ink - substrate interaction

The interaction between the ink and the substrate before sintering was investigated by measuring the surface tension of the ink, the surface energy of the substrates and the CA of the ink on the substrates. The average surface tension of the AgNP ink was measured as 28.7 mN/m. The surface energy (γ^{tot}), dispersive component (γ^{d}) and polar component (γ^{p}) for CNF, ACNF and CRM substrates are displayed in Table 1.

The surface energy is much lower for CNF compared to ACNF, due to the significantly higher polar component for ACNF. Acetylated cellulose is usually more hydrophobic and has a lower polarity compared to untreated cellulose [42–45]. However; sodium hydroxide (NaOH) treatment has been shown to increase the polarity of cellulose [46]. The use of NaOH to adjust the pH of the ACNF was deduced to be the main reason for the increase in the polarity [47]. It should be noted that the dispersive component is still higher for ACNF compared to the polar component.

Moreover, the dispersive component of CRM [48] is higher compared to CNF and ACNF, however; the total surface energy of CRM is quite similar to ACNF. In addition, the ratios between dispersive or polar components in comparison to the total surface energy are clearly different for the ACNF (higher polar share and lower dispersive share) compared to the other substrates.

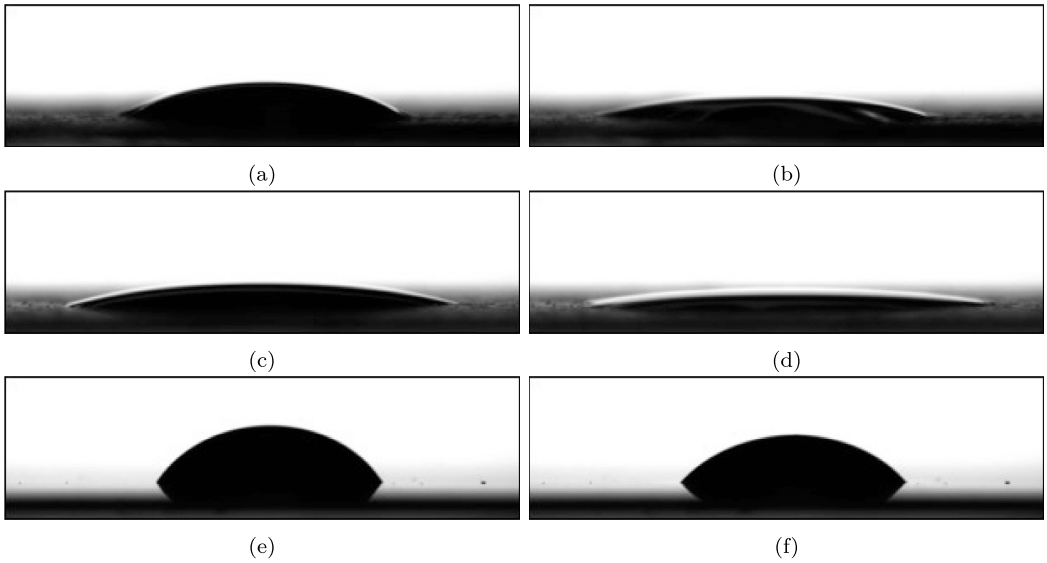

Fig. 1. Initial (a, c, e) and final (b, d, f) CAs of AgNP on CNF (a, b), ACNF (c, d) and CRM (e, f).

The initial (t = 0 s) and final (t = 300 s) CAs for the AgNP ink on CNF, ACNF and CRM substrates are also displayed in Table 1 and Fig. 1. The initial and final CAs for the ink are the largest for the CRM substrate whilst the smallest for the ACNF substrate. ACNF and CRM have similar surface energy, yet the CA is significantly lower for the ink on the ACNF substrate compared to the CRM substrate. As explained by Wiklund et al. [1], a higher surface roughness can increase the wetting and decrease the CA of the ink on the substrate if the CA is lower than 90°. The RMS height of the ACNF and CRM substrates are 1.5 μm and 0.8 μm, respectively. Additionally, higher porosity for CNF and ACNF substrates cause a higher absorption of the ink. However, the change in CA during the 5 minute (t = 300 s) experiment is the smallest for ACNF and the largest for CNF. This means that the wetting of the ink on the ACNF substrate is instant, while the change in CA advances with the solvent evaporation and absorption. On the other hand, the change in CA for CRM can be explained in terms of the spreading of the ink and solvent evaporation.

3.2. Print quality

The print quality was examined by measuring the width, thickness, RMS height, and hole area fraction of the printed pattern on the substrate. The measured width of the printed pattern is wider than the desired printed width. This difference in width is due to the spreading of the ink on the substrate. In Fig. 2a spreading of the ink for 1-4 layers of ink on CNF, ACNF and CRM is displayed.

The printed pattern on CRM substrate show significantly more spreading compared to CNF and ACNF, which could be related with the larger absorption rates of the ink on CNF and ACNF. Additionally, the smoother surface of CRM could allow for the ink to spread more easily. The spreading of the ink on the CRM substrate is approximately the same (≈0.5 mm) for 1, 2, 3 or 4 layers of ink, which means that the additional layers of ink do not display any more spreading compared to the first layer. The explanation for this is that the spreading of the ink on the CRM substrate occurs during the sintering process.

The spreading of the ink on the ACNF substrate is mostly the smallest and it increased slightly for each additional layer of ink. This could be explained by a partial absorption of the ink into the pores [49] of the ACNF film for the first ink layer, which allows for more spreading of the ink for every subsequent ink layer. The larger fibers in the CNF film compared to the ACNF film [50,28] results in less homogeneous substrates, which makes the spreading of the ink more unpredictable.

Fig. 2b shows optical microscope images of 0.1 mm wide printed pattern on CNF, ACNF and CRM substrates with 1-4 layers. The printed pattern on CNF is clearly less uniform than the printed patterns on ACNF and CRM. When printing 4 layers of ink on CNF and ACNF substrates a small separate line can be seen parallel to the printed pattern. This line becomes more visible for each printed layer and it is caused by satellite droplets. These satellite droplets are not visible on the CRM substrate, because the significant spreading of the ink, which covers them.

The thicknesses of the layers of ink on ACNF and CRM substrates are displayed in Fig. 3a. The thickness of the ink pattern on the ACNF substrate is 4 μm and it increases by approximately 1.6 μm with each additional ink layer. For the ink pattern on the CRM substrate, the first ink layer is significantly thicker compared to the ink layer on the ACNF substrate, 5.7 μm. This difference can be explained by the partial absorption of the ink into the ACNF substrate. Interestingly, the increase in thickness for each subsequent ink layer is subsiding on the CRM substrate.

In Fig. 3b, the RMS height and hole area fraction of the ink layers on the ACNF and CRM substrates are displayed. The RMS height of the ink layers on the CRM substrate are around 2 ±0.25 μm regardless of the amount of layers. For the ACNF substrate, the RMS height of one ink layer was 2.9 μm and it increased for each subsequent layer, reaching 4.3 μm for 4 layers. The RMS height is higher for the ACNF substrate compared to the CRM substrate, the ink layers on the substrate intensify the RMS height of the substrate itself.

The hole area fraction of the printed pattern on the ACNF substrate decreases with every subsequent layer of ink, from 33% to 13%. The holes in the ink layers can be caused, e.g. by absorption of the NPs into the pores of the substrate. This is due to each additional ink layer covering some of the holes left by the previous layer. For instance, the ink layers on the CRM substrate have a hole area fraction of 14% for one ink layer while it is only 4% for four ink layers.

3.3. Electrical properties

The electrical properties were studied by measuring the relative permittivity of the ACNF substrate, and the resistance and sheet resistance of the printed patterns on the substrates. The measured resistance of the printed test patterns on CNF, ACNF and CRM with 1-4 layers of ink are presented in Fig. 4. The resistance decreases significantly by increasing the amount of ink layers used on ACNF and CRM. However, it was not possible to get any values for the patterns on CNF substrate with 1-3

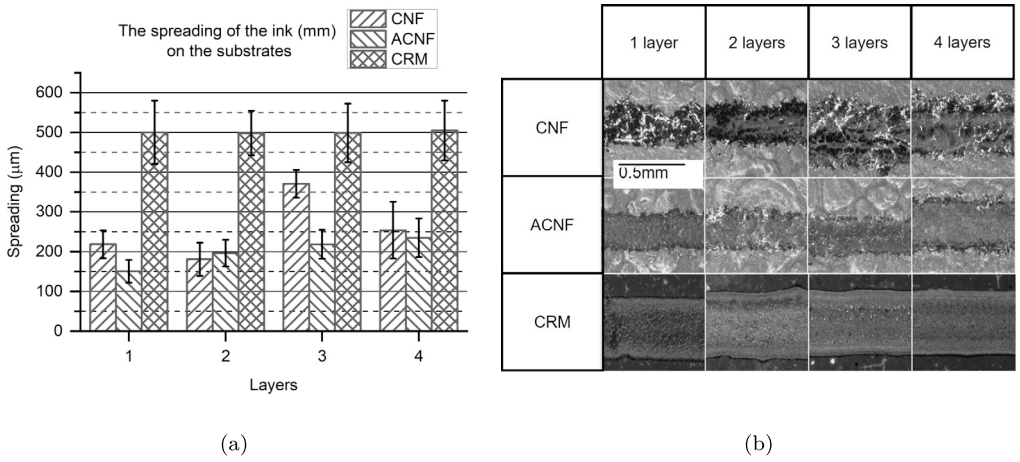

Fig. 2. (a) The spreading of the ink for 1-4 layers of ink on CNF, ACNF and CRM. (b) Microscopy images of 0.1 mm wide printed pattern on CNF, ACNF and CRM with 1-4 layers.

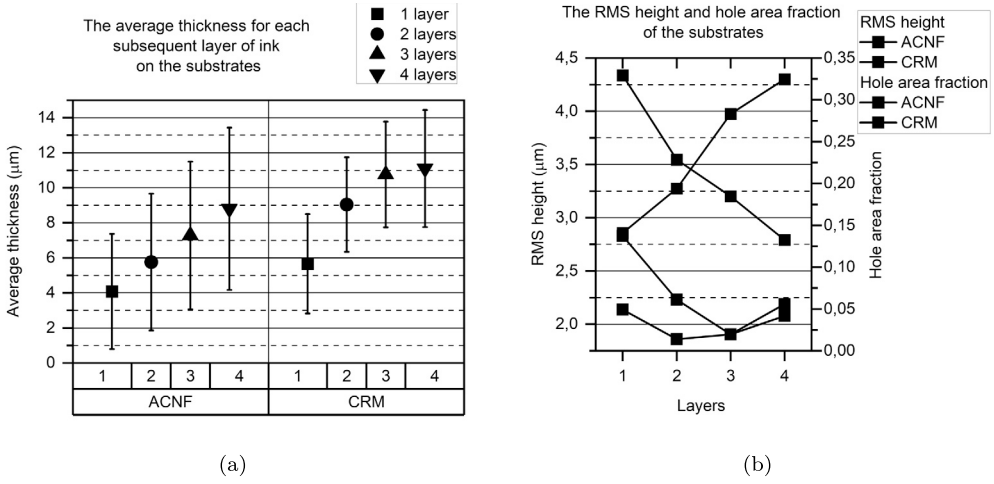

Fig. 3. (a) The thickness of the layers of ink on ACNF and CRM substrates. (b) The root mean squared (RMS) height and hole area fraction of the printed layers on ACNF and CRM substrates.

layers of ink and the resistance for 4 layers of ink on the CNF substrate is 5 $M\Omega$. This is mostly due to the absorption of the NPs and the higher surface roughness. If the ink particles are not connected after sintering across the pattern, it is not possible to measure the resistance. Using 4 layers of ink, the resistance achieved was 1.2 Ω and 1.6 Ω for CRM and ACNF, respectively. The mean sheet resistance for four layers of ink on the ACNF and CRM substrates were 11 ±0.3 mΩ/sq and 7 ±0.5 mΩ/sq, respectively.

The mean value of the relative permittivity ε_r of the ACNF substrate was calculated as 13.2 over the frequency range of 2-6 GHz. The value was obtained by considering the measured effective permittivity ε_{eff} of CPW transmission lines printed on the substrate. ε_{eff} between 2-6 GHz was 1.70 with a standard deviation of 0.07. This variation yields a range of 12.0-14.5 for the relative permittivity of the substrate. Moreover, considering a total of ±1 mm positioning error in the placement of measurement probes on the samples yields a possible range of 1.61-1.78 and 11.7-14.6 for the mean values of ε_{eff} and ε_r, respectively. It is important to note that the relative permittivity value is applicable for the printed CPW transmission lines on the substrate. Due to possible anisotropy of permittivity, the results may differ depending on the orientation of electric fields in the material when used with a different method of measurement or application.

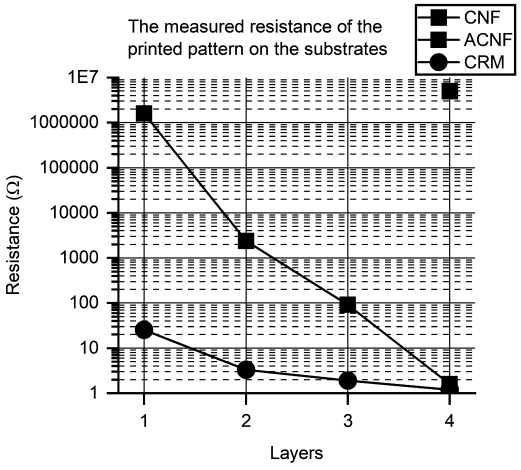

Fig. 4. The measured resistance for the printed pattern on CNF, ACNF and CRM with 1-4 layers of AgNP ink.

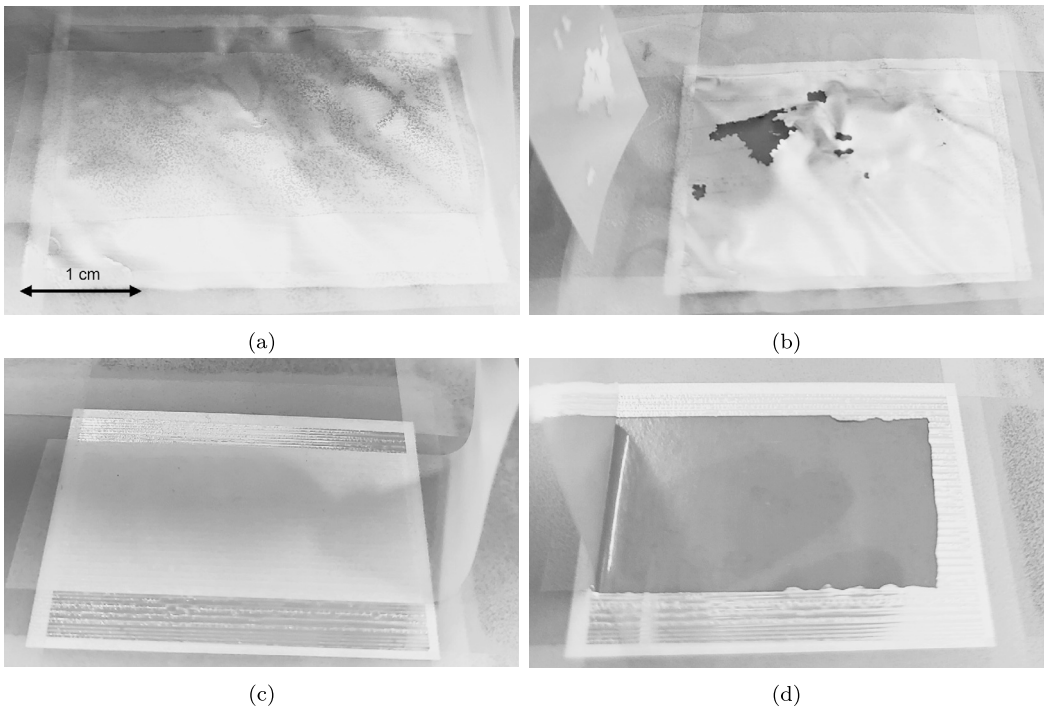

Fig. 5. The printed pattern on the ACNF substrate (a) before and (b) after the adhesion test, (c) before and (d) after the adhesion test for the printed pattern on the CRM substrate.

3.4. Mechanical properties

The mechanical properties of the printed patterns on the substrates were investigated by testing the adhesion and bending resistance. The adhesion of the ink on the CRM substrate was significantly less compared to the ACNF substrate, as can be seen from Fig. 5. The sheet resistance was not possible to be measured after the adhesion test due the ink layers being completely removed by the tape from the CRM substrate. The ACNF showed much higher adhesion with only one larger area and otherwise smaller areas ($< 1mm$) of the ink layer being removed by the tape. The sheet resistance remained approximately the same after the adhesion test. The better adhesion characteristics between the ink and the ACNF substrate can be explained by the rougher surface and higher porosity. When printing, part of the ink fill the small pores in the ACNF film, which makes the ink-ACNF substrate interface harder to be separated compared to the one with a smooth surface without pores. A high surface roughness and porosity can on the other hand cause cracking and discontinuities in the printed pattern [9]. Both of these aspects need to be taken into account, when designing a substrate for printed electronics. The choice depends on the application and the environmental requirements of the printed device.

There was no change in the resistance for the printed patterns on neither the ACNF nor the CRM after 10 bending resistance measurements using 30° angle. Nonetheless, after changing the angle to 90°, the adhesion started to fail for the CRM and the resistivity was not possible to measure after an average of additional 13 bending cycles. In addition, the resistivity for the ACNF samples also started to slowly increase after several measurements.

The ACNF film would make a great substrate for printed electronics, considering the excellent results of this study. These include the instant wetting of the AgNP ink on the ACNF substrate, in addition to, the remarkably good quality, resistance, adhesion and bending resistance of the printed AgNP pattern on the ACNF substrate.

4. Conclusions

In the present study, the suitability of ACNF substrates for printed electronics was investigated. For this objective, the interaction between the AgNP ink and ACNF substrate, print quality, electrical and mechanical properties were examined in detail. The results were compared to the ones measured for the ink on CNF and/or CRM substrates, when applicable. The wetting of the ink on the ACNF substrate was deduced to be very good while the CA was very small and did not decrease much during the experiment. The print quality achieved on the ACNF substrate was determined to be high through comprehensive analysis of ink spreading characteristics. It is here noteworthy that pattern designs in printed electronics need careful considerations of the ink spreading to minimize the gap between the design and actual device. Moreover, the electrical properties of the printed pattern on the ACNF film (1.6 Ω resistance) were almost as good as the one for the CRM substrate (1.2 Ω resistance), especially when printing four layers of ink. Furthermore, the mechanical characterisation of the printed pattern on the ACNF substrate were significantly better when compared with the ones for the CRM substrate. The results of this investigation demonstrate that ACNF can be used as a reliable and sustainable substrate for printed electronics with careful considerations of the spreading of the ink during the design stage and the use of enough layers of ink during the printing stage. Due to the time-consuming and laborious manufacturing process of ACNF films, mass production using this method would be difficult at this stage. Additionally, if the environment where the printed device is used in is very humid, the printed pattern will dissolve. In order to protect the device, lamination process would be required. If these limitations would be overcome, inkjet printing electronics onto ACNF substrates would both reduce the use of non-renewable materials and simplify the recycling of the electronic waste, compared to the electronics produced using the traditional subtractive technique on fossil-based substrates. Additionally, this method of producing printed electronics enables the production of prototypes and small batches for a relatively low cost in comparison with other methods.

CRediT authorship contribution statement

Jenny Wiklund: Writing – review & editing, Writing – original draft, Visualization, Validation, Supervision, Resources, Project administration, Methodology, Investigation, Funding acquisition, Formal analysis, Data curation, Conceptualization. **Arttu Miettinen:** Writing – review & editing, Writing – original draft, Visualization, Validation, Resources, Investigation, Formal analysis, Data curation. **Joni Parkkonen:** Writing – original draft, Visualization, Resources, Investigation, Formal analysis, Data curation. **Lauri Mela:** Writing – review & editing, Writing – original draft, Validation, Resources, Investigation, Formal analysis, Data curation. **Alp Karakoç:** Writing – review & editing, Visualization, Validation, Supervision, Project administration, Funding acquisition, Conceptualization. **Jouni Paltakari:** Writing – review & editing, Visualization, Validation, Supervision, Resources, Project administration, Funding acquisition, Conceptualization.

Declaration of competing interest

The authors declare that they have no known competing financial interests or personal relationships that could have appeared to influence the work reported in this paper.

Data availability

Data will be made available on request.

Funding

J.W. acknowledges the funding from Jenny and Antti Wihuri Foundation. The funding through Academy of Finland BESIMAL (Decision No. 334197) and WALLPAPER (Decision No. 352912) projects are also acknowledged.

References

[1] J. Wiklund, A. Karakoç, T. Palko, H. Yiğitler, K. Ruttik, R. Jäntti, J. Paltakari, A review on printed electronics: fabrication methods, inks, substrates, applications and environmental impacts, J. Manuf. Mater. Process. 5 (2021) 89.

[2] J. Kerminen, J. Wiklund, A. Karakoç, K. Ruttik, R. Jäntti, H. Yiğitler, Characterization of low-cost inkjet printed-photonic cured strain gauges for remote sensing and structural monitoring applications, Res. Eng. Struct. Mater. 7 (2021) 647–660.

[3] E. Kunnari, J. Valkama, M. Keskinen, P. Mansikkamäki, Environmental evaluation of new technology: printed electronics case study, J. Clean. Prod. 17 (2009) 791–799.

[4] W. Wu, Inorganic nanomaterials for printed electronics: a review, Nanoscale 9 (2017) 7342–7372.

[5] J. Perelaer, P.J. Smith, D. Mager, D. Soltman, S.K. Volkman, V. Subramanian, J.G. Korvink, U.S. Schubert, Printed electronics: the challenges involved in printing devices, interconnects, and contacts based on inorganic materials, J. Mater. Chem. 20 (2010) 8446–8453.

[6] J. Kerminen, B. Xie, L. Mela, A. Karakoç, K. Ruttik, R. Jäntti, Low-cost thin film patch antennas and antenna arrays with various background wall materials for indoor wireless communications, Flexible and Printed Electronics, http://iopscience.iop.org/article/10.1088/2058-8585/accd05, 2023.

[7] S.-W. Hwang, H. Tao, D.-H. Kim, H. Cheng, J.-K. Song, E. Rill, M.A. Brenckle, B. Panilaitis, S.M. Won, Y.-S. Kim, et al., A physically transient form of silicon electronics, Science 337 (2012) 1640–1644.

[8] X. Han, K.J. Seo, Y. Qiang, Z. Li, S. Vinnikova, Y. Zhong, X. Zhao, P. Hao, S. Wang, H. Fang, Nanomeshed si nanomembranes, npj Flex. Electron. 3 (2019) 1–8.

[9] F. Hoeng, A. Denneulin, J. Bras, Use of nanocellulose in printed electronics: a review, Nanoscale 8 (2016) 13131–13154.

[10] M.J. Tan, C. Owh, P.L. Chee, A.K.K. Kyaw, D. Kai, X.J. Loh, Biodegradable electronics: cornerstone for sustainable electronics and transient applications, J. Mater. Chem. C (2016), https://doi.org/10.1039/c6tc00678g.

[11] Y. Wang, S. Lee, T. Yokota, H. Wang, Z. Jiang, J. Wang, M. Koizumi, T. Someya, A durable nanomesh on-skin strain gauge for natural skin motion monitoring with minimum mechanical constraints, Sci. Adv. 6 (2020) eabb7043.

[12] B. Wang, A. Thukral, Z. Xie, L. Liu, X. Zhang, W. Huang, X. Yu, C. Yu, T.J. Marks, A. Facchetti, Flexible and stretchable metal oxide nanofiber networks for multimodal and monolithically integrated wearable electronics, Nat. Commun. 11 (2020) 1–11.

[13] K.D. Misic, A. Karakoc, M. Ozkan, S.G. Hashmi, T. Maloney, J. Paltakari, Flow characteristics of ink-jet inks used for functional printing, J. Appl. Eng. Sci. 13 (2015).

[14] S. Agate, M. Joyce, L. Lucia, L. Pal, Cellulose and nanocellulose-based flexible-hybrid printed electronics and conductive composites–a review, Carbohydr. Polym. 198 (2018) 249–260.

[15] P. Ihalainen, A. Maattanen, J. Jarnstrom, D. Tobjork, R. Osterbacka, J. Peltonen, Influence of surface properties of coated papers on printed electronics, Ind. Eng. Chem. Res. 51 (2012) 6025–6036.

[16] S. Ahmad, K. Rahman, M. Shakeel, T.A.K. Qasuria, T.A. Cheema, A. Khan, A low-cost printed humidity sensor on cellulose substrate by ehd printing, J. Mater. Res. 36 (2021) 3667–3678.

[17] Z. Gozutok, O. Kinj, I. Torun, A.T. Ozdemir, M.S. Onses, One-step deposition of hydrophobic coatings on paper for printed-electronics applications, Cellulose 26 (2019) 3503–3512.

[18] Y. Ko, G. Kwon, H. Choi, K. Lee, Y. Jeon, S. Lee, J. Kim, J. You, Cutting edge use of conductive patterns in nanocellulose-based green electronics, Adv. Funct. Mater. 33 (2023) 2302785.

[19] Y.H. Jung, T.-H. Chang, H. Zhang, C. Yao, Q. Zheng, V.W. Yang, H. Mi, M. Kim, S.J. Cho, D.-W. Park, et al., High-performance green flexible electronics based on biodegradable cellulose nanofibril paper, Nat. Commun. 6 (2015) 1–11.

[20] M. Özkan, A. Karakoç, M. Borghei, J. Wiklund, O.J. Rojas, J. Paltakari, Machine learning assisted design of tailor-made nanocellulose films: a combination of experimental and computational studies, Polym. Compos. 40 (2019) 4013–4022.

[21] T. Abitbol, A. Rivkin, Y. Cao, Y. Nevo, E. Abraham, T. Ben-Shalom, S. Lapidot, O. Shoseyov, Nanocellulose, a tiny fiber with huge applications, Curr. Opin. Biotechnol. 39 (2016) 76–88.

[22] L.G. Greca, M. Rafiee, A. Karakoç, J. Lehtonen, B.D. Mattos, B.L. Tardy, O.J. Rojas, Guiding bacterial activity for biofabrication of complex materials via controlled wetting of superhydrophobic surfaces, ACS Nano 14 (2020) 12929–12937.

[23] G. Lo Re, S. Spinella, A. Boujemaoui, F. Vilaseca, P.T. Larsson, F. Adås, L.A. Berglund, Poly (ϵ-caprolactone) biocomposites based on acetylated cellulose fibers and wet compounding for improved mechanical performance, ACS Sustain. Chem. Eng. 6 (2018) 6753–6760.

[24] J. Wohlert, P. Chen, L.A. Berglund, G. Lo Re, Acetylation of nanocellulose: miscibility and reinforcement mechanisms in polymer nanocomposites, ACS Nano (2023).

[25] K. Missoum, M.N. Belgacem, J. Bras, Nanofibrillated cellulose surface modification: a review, Materials 6 (2013) 1745–1766.

[26] S. Rodríguez-Fabià, J. Torstensen, L. Johansson, K. Syverud, Hydrophobization of lignocellulosic materials part ii: chemical modification, Cellulose 29 (2022) 8957–8995.

[27] H. Yagyu, S. Ifuku, M. Nogi, Acetylation of optically transparent cellulose nanopaper for high thermal and moisture resistance in a flexible device substrate, Flex. Print. Electron. 2 (2017) 014003.

[28] S. Yang, Q. Xie, X. Liu, M. Wu, S. Wang, X. Song, Acetylation improves thermal stability and transmittance in foled substrates based on nanocellulose films, RSC Adv. 8 (2018) 3619–3625.

[29] V. Zepič, I. Poljanšek, P. Oven, A.S. Škapin, A. Hančič, Effect of drying pretreatment on the acetylation of nanofibrillated cellulose, BioResources 10 (2015) 8148–8167.

[30] A. James, M.R. Rahman, K.A. Mohamad Said, D. Kanakaraju, A.Z. Sueraya, K.K. Kuok, M.K. Bin Bakri, M.M. Rahman, A review of nanocellulose modification and compatibility barrier for various applications, J. Thermoplast. Compos. Mater. 37 (2024) 2149–2199.

[31] K.-M. Chin, S. Sung Ting, H.L. Ong, M. Omar, Surface functionalized nanocellulose as a veritable inclusionary material in contemporary bioinspired applications: a review, J. Appl. Polym. Sci. 135 (2018) 46065.

[32] A. Ashori, M. Babaee, M. Jonoobi, Y. Hamzeh, Solvent-free acetylation of cellulose nanofibers for improving compatibility and dispersion, Carbohydr. Polym. 102 (2014) 369–375.

[33] R. Ajdary, S. Huan, N. Zanjanizadeh Ezazi, W. Xiang, R. Grande, H.A. Santos, O.J. Rojas, Acetylated nanocellulose for single-component bioinks and cell proliferation on 3d-printed scaffolds, Biomacromolecules 20 (2019) 2770–2778.

[34] J. Gigac, M. Fišerová, M. Kováč, M. Stankovská, Paper substrates for inkjet printing of uhf rfid antennas, Wood Res. 65 (2020) 25–36.

[35] B. Le Borgne, B.-Y. Chung, M.O. Tas, S.G. King, M. Harnois, R.A. Sporea, Eco-friendly materials for daily-life inexpensive printed passive devices: towards “do-it-yourself” electronics, Electronics 8 (2019) 699.

[36] S. Mohassieb, K. Kirah, E. Dörsam, A.S. Khalil, H.M. El-Hennawy, Effect of silver nanoparticle ink drop spacing on the characteristics of coplanar waveguide monopole antennas printed on flexible substrates, IET Microw. Antennas Propag. 11 (2017) 1572–1577.

[37] C. Chiappara, V. Campisciano, G. Arrabito, V. Errico, G. Saggio, G. Buscarino, M. Scopelliti, M. Gruttadauria, F. Giacalone, B. Pignataro, Bending sensors based on thin films of semitransparent bithiophene-fulleropyrrolidine bisadducts, ChemPlusChem 85 (2020) 2455–2464.

[38] Z. Deng, B. Rosales, L. Choi, S. Mooers, B.C. Johnson, 3d-printed and wireless piezoelectric tactile sensors, in: Electroactive Polymer Actuators and Devices (EAPAD) XXII, Volume 11375, International Society for Optics and Photonics, 2020, p. 113752A.

[39] K. Ton, T.-Y. Chu, Z. Zhang, Y. Tao, Printing contractive silver conductive inks using interface interactions to overcome dewetting, IEEE J. Electr. Dev. Soc. 7 (2019) 756–760.

[40] T. Turpeinen, M. Myllys, K. Pekka, J. Timonen, Interface detection using a quenched-noise version of the Edwards–Wilkinson equation, IEEE Trans. Image Process. 24 (2015) 5696–5705.
[41] N.K. Das, S.M. Voda, D.M. Pozar, Two methods for the measurement of substrate dielectric constant, IEEE Trans. Microw. Theory Tech. 35 (1987), https://doi.org/10.1109/TMTT.1987.1133722.
[42] A.M. Stepan, F. Ansari, L. Berglund, P. Gatenholm, Nanofibrillated cellulose reinforced acetylated arabinoxylan films, Compos. Sci. Technol. 98 (2014) 72–78.
[43] S. Lin, J. Huang, P.R. Chang, S. Wei, Y. Xu, Q. Zhang, Structure and mechanical properties of new biomass-based nanocomposite: castor oil-based polyurethane reinforced with acetylated cellulose nanocrystal, Carbohydr. Polym. 95 (2013) 91–99.
[44] Y. Xu, W. Ding, J. Liu, Y. Li, J.F. Kennedy, Q. Gu, S. Shao, Preparation and characterization of organic-soluble acetylated starch nanocrystals, Carbohydr. Polym. 80 (2010) 1078–1084.
[45] X. Zhou, X. Lin, K.L. White, S. Lin, H. Wu, S. Cao, L. Huang, L. Chen, Effect of the degree of substitution on the hydrophobicity of acetylated cellulose for production of liquid marbles, Cellulose 23 (2016) 811–821.
[46] H. Dhakal, Z. Zhang, N. Bennett, Influence of fibre treatment and glass fibre hybridisation on thermal degradation and surface energy characteristics of hemp/unsaturated polyester composites, Composites, Part B, Eng. 43 (2012) 2757–2761.
[47] K. Indira, Y. Grohens, C. Baley, S. Thomas, K. Joseph, L. Pothen, Adhesion and wettability characteristics of chemically modified banana fibre for composite manufacturing, J. Adhes. Sci. Technol. 25 (2011) 1515–1538.
[48] P. Suly, J. Sevcik, D.J. Dmonte, P. Urbanek, I. Kuritka, Inkjet printability assessment of weakly viscoelastic fluid: a semidilute polyvinylpyrrolidone solution ink case study, Langmuir 37 (2021) 8557–8568.
[49] S. Merilampi, T. Laine-Ma, P. Ruuskanen, The characterization of electrically conductive silver ink patterns on flexible substrates, Microelectron. Reliab. 49 (2009) 782–790.
[50] M. Jonoobi, J. Harun, A.P. Mathew, M.Z.B. Hussein, K. Oksman, Preparation of cellulose nanofibers with hydrophobic surface characteristics, Cellulose 17 (2010) 299–307.